Optics Communications 331 (2014) 348–352

Contents lists available at ScienceDirect

Optics Communications

journal homepage: www.elsevier.com/locate/optcom

Fiber-optic Michelson interferometer with high sensitivity based on a liquid-filled photonic crystal fiber

Jui-Ming Hsu, Jing-Shyang Horng, Chia-Ling Hsu, Cheng-Ling Lee *

Department of Electro-Optical Engineering, National United University, No.1 Lien-Da, Kung-Ching Li, Miaoli 360, Taiwan, ROC

ARTICLE INFO

Article history:
Received 3 April 2014
Received in revised form
23 June 2014
Accepted 24 June 2014
Available online 3 July 2014

Keywords:
Liquid-filled photonic crystal fiber
Michelson interferometer (LF-PCFMI)
Photonic crystal fiber interferometer (PCFI)
Photonic crystal fiber (PCF)
Material dispersion engineering

ABSTRACT

This study proposes an ultracompact and highly sensitive liquid-filled photonic crystal fiber Michelson interferometer (LF-PCFMI) based on material dispersion engineering. Numerical simulations and experimental measurements are performed in the work, and both of their results show that the temperature sensitivity can be more greatly improved than those of conventional photonic crystal fiber interferometers (PCFIs). The experimental results indicate that a very high sensitivity with interference wavelength shifts of almost 27 nm within temperature variation of 5 °C has been achieved by the configuration. Numerical analysis for the proposed LF-PCFMI also exhibits a good agreement with the results of the experimental measurements.

1. Introduction

Photonic crystal fiber interferometers (PCFIs) with superiority of the unique-material fiber structure have been extensively developed as all-fiber based strain ($\mu\varepsilon$) [1], external refractive index (RI) [2], bending [3] and temperature (T) [4] sensors. The majority of the meritorious applications of PCFIs on the fiber-optic sensing are all accredited to the structure of cyclic air voids in the photonic crystal fiber (PCF) which attracts considerable attention of researchers. The commercial PCF is fabricated with pure silica; therefore filling other material with different optical properties into an available PCF is a good method to vary the characteristics of propagation modes in the PCF and achieves a flexible design. Many studies about filling the air holes of PCFs with different materials for ultrasensitive sensing applications have been proposed [5–9], like fiber Mach–Zehnder interferometers [4–6], fiber Fabry–Perot interferometer [7] and selectively liquid-filled PCF [8]. Hu Liang et al. filled liquid (with a refractive index approximating silica fiber) in one hole of the innermost layer of a photonic crystal fiber. The ellipse-like core brought about a high order mode with different optical path length with the core mode; consequently achieve a fiber Mach–Zehnder interferometer [6]. A photonic bandgap fiber (PBGF) can be implemented by infusing liquid (with a refractive index higher than the core) into all the cladding holes of the index-guided photonic crystal fiber. Han et al. spliced a section of Fabry–Perot interferometer between the above-mentioned PBGF and a single mode fiber to achieve a novel fiber Fabry–Perot interferometer for simultaneously measuring force and temperature [7]. Another study, Peng, et al. filled a high-index liquid with high thermo-optic coefficient into the first ring around the core of PCF based on the bandgap-like effect to obtain a highly sensitive temperature sensor [8]. A highly sensitive temperature sensor that is based on an alcohol-filled PCF with the PCF length of 6.1 cm has been also proposed [9]. Other liquid, the well known liquid crystal also can be filled into the PCFs and have been presented for many electrically tunable fiber-optic devices: for example, a fiber polarimeter [10], a directional electrical field fiber sensor [11], a tunable fiber Sagnac filter [12] and a fiber-optic switch [13]. Based on the results of the above studies, filling other materials into air-holes of the commercial PCFs is a simple way to achieve the novel and flexible design for the PCF-based devices.

In this paper, we develop an ultrasensitive, ultracompact, tip typed, in-line liquid-filled photonic crystal fiber Michelson interferometer (LF-PCFMI) based on the material dispersion engineering. The sensor tip is composed of a single mode fiber (SMF) splicing with a small section of index-guiding photonic crystal fiber. Fig. 1(a) presents the configuration of proposed LF-PCFMI. Fig. 1(b) and (c) indicates the micrographs of the PCF (LMA-8) tips without and with filled-liquid, respectively. The air-voids of the PCF were fully collapsed in the splicing process and resulted in a collapsed region with about a length of 300 μm between SMF and PCF. Here, the Ericsson FSU-975 commercial fusion splicer was used with discharge duration of 8.5 seconds and current of 10 mA to destroy the air holes in cladding of the PCF. The insertion loss by

* Corresponding author. Tel.: +886 37 381732; fax: +886 37 351575.
E-mail address: cherry@nuu.edu.tw (C.-L. Lee).

http://dx.doi.org/10.1016/j.optcom.2014.06.050
0030-4018/

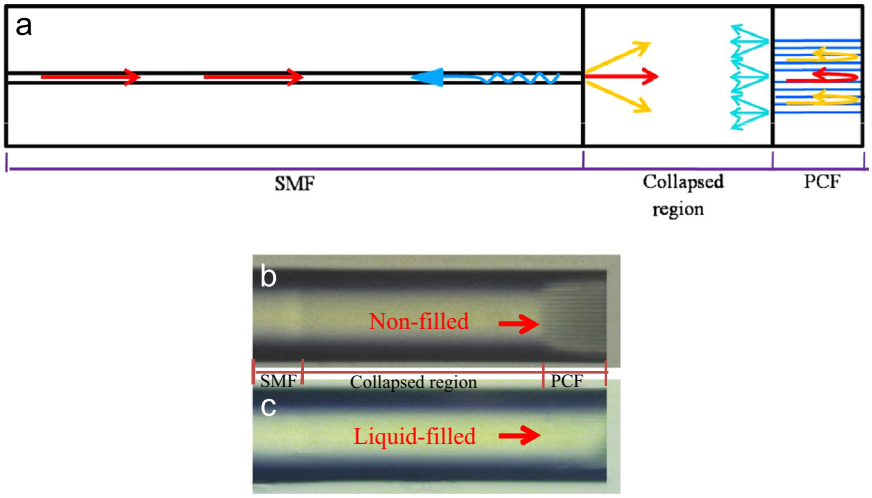

Fig. 1. (a) Configuration of the proposed LF-PCFMI. Photographs of the LF-PCFMI sensor tips with the (b) non-filled, and (c) liquid-filled conditions, respectively.

the splicing process is about 3–4 dB in the case. Afterward, by cleaving the end of the PCF, we can fabricate the LF-PCFMI sensor tip with an arbitrary length of PCF. The collapsed region is not a guiding fiber anymore that acts like a multimode fiber since the section has no guiding core. Therefore, the fundamental SMF mode begins to diffract when it enters the collapsed region and excites several high-order cladding modes, these high-order modes then penetrate into the PCF section. The core mode and cladding modes are reflected by the PCF endface and interfere with each other in the collapsed region at their return trip.

The light propagating in the cladding can be engineered by filling material into the air holes for enhancing sensitivity. As everyone knows that the silica-based sensors exhibit low temperature sensitivity due to a very low thermal expansion coefficient (TEC) of about $5.5\times10^{-7}\,^{\circ}C^{-1}$ and low thermo-optics coefficient (TOC) of about $5\times10^{-6}\,^{\circ}C^{-1}$. Thus, we can make the air holes in the cladding of PCF fully filled with Cargille® optical liquid by duration of the capillary action. Because the TOC of the filled liquid of $dn/dT=-3.74\times10^{-4}\,^{\circ}C^{-1}$ is much larger than those of the silica and air, the temperature-caused variation of the chromatic dispersion in the cladding of filled-liquid PCF is stronger than that of ordinary PCF. Therefore, the effective indices (n_{eff}) of the cladding modes are greatly varied with the temperature that is indicated an enhancement of the tuning efficiency of the proposed liquid-filled PCF-sensors.

2. Numerical results and analysis

Some simulation work has been accomplished to theoretically analyze the behaviors of light propagating in the proposed LF-PCFMI device. To elucidate the mode expansion in the collapsed region, the field distribution can be simulated by using the finite difference beam propagation method, as shown in Fig. 2(a) and (b). The parameters of the simulation model were set as follows: the lengths of the SMF, collapsed region, and PCF are 100 μm, 300 μm, and 31.3 μm, respectively. The light beam expands in the collapsed region and penetrates into the PCF section as mentioned above which is clearly shown in Fig. 2.

Fig. 3(a) and (b) respectively shows the mode pattern distribution at the PCF endface before and after filled Cargille optical liquid with of refractive index (RI) $n_D=1.45$. Here the n_D value of the used Cargille index oil are measured at 25 °C, Sodium D Line, and $\lambda=589.3$ nm. In the non-liquid-filled case shown in Fig. 3(a), optical power mainly gathers around the solid silica of PCF, but it disperses into the liquid rods after liquid-filling that is plotted in Fig. 3(b).

The optical liquid with the TOC, $dn/dT=-3.74\times10^{-4}\,^{\circ}C^{-1}$ is more dispersive corresponding to the temperature than the air, therefore it can be predicted that the effective indices can be greatly modulated by varying the temperature. Fig. 4(a) and (b) shows the calculated effective indices (n_{eff}^{m}) of the three lowest modes for the proposed device before and after filling with optical liquid, respectively. In Fig. 4(b), the cladding holes of PCF filled liquid with $n_D=1.45$ whose refractive index (RI) approaches to those of the silica, thus the nominal core mode is almost vanished. Accordingly, the n_{eff}^{m} curves are denoted as mode 1, 2, 3 instead of core and cladding modes. Inset of Fig. 4(b) indicates the clear n_{eff}^{m} curves of the mode 1, 2 and 3, respectively. The effective indices of three lowest modes are considerably increased and assembled in around the value of 1.4430–1.4435 within the wavelength range of 1200 nm to 1600 nm. For the liquid-filled condition, as shown in Fig. 4(b), the index of the liquid dominates the effective indices of the modes; therefore a higher temperature sensitivity of the liquid may dominates the sensitive performances of the sensor as well.

Fig. 5 shows variations of the effective indices for the two lowest modes (mode 1 and 2) in liquid-filled ($n_D=1.45$) situation when the temperature changes. The effective indices greatly decrease with temperature due to the negative and high TOC of the used liquid. In this regard, optical spectra of the modal interference of the proposed device would be strongly modulated by temperature and can achieve a highly sensitive temperature sensor.

To compare the temperature sensitivity between the effective indices of mode 1 and mode 2, the dependence of differential effective indices for the mode 1 and mode 2 corresponding to the temperature at a fixed wavelength (λ) of 1500 nm are estimated and indicated in Fig. 6. The numerical result reveals that the differential effective indices to the temperature of mode 1 and mode 2 are both negative and the effective index decrease with the increased temperature for the mode 1 is larger than that of mode 2.

The theoretical analysis about the spectral response of the wavelength shifting in the LC-PCFMI is performed as follows. In the case the excitation and recombination of the interference modes are respectively achieved at the same collapsed region between SMF and PCF. The interference mechanism of the proposed configuration is two-mode (which are denoted as mode 1 and mode 2 with intensities of I_{m1}, and I_{m2} respectively) interference due to the weak interference intensities of the modes. Thus, the intensity of the modal interference fringes can be easily expressed as:

$$I_{total}=I_{m1}+I_{m2}+2\sqrt{I_{m1}I_{m2}}\,\cos(\Phi) \tag{1}$$

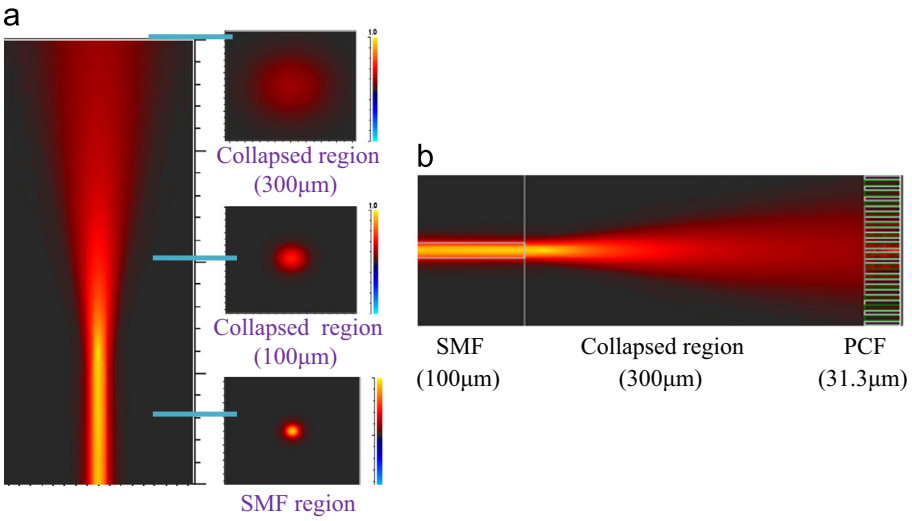

Fig. 2. Simulation results for (a) the evolution of field distributions in the SMF and collapsed region, (b) mode expansion in the LF-PCFMI device with a collapsed region of 300 μm and a PCF length of 31.3 μm.

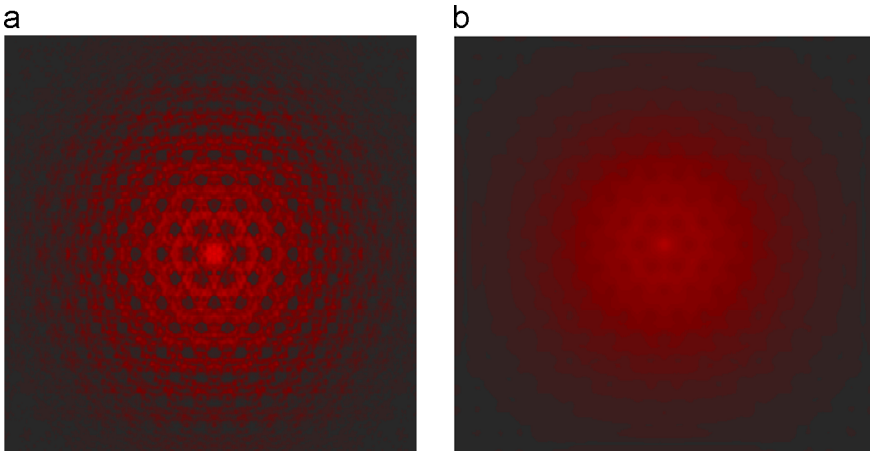

Fig. 3. Mode distributions in the PCF endface for the (a)non-filled, and (b) liquid-filled conditions, respectively.

The optical phase difference between the two modes $\Phi = (2\pi/\lambda)\cdot(\mathrm{OPD})$, where $\mathrm{OPD} = \Delta n_{\mathrm{eff}}^{\mathrm{m}} 2L$ is the optical path difference. λ denotes the wavelength. Here L is the liquid-filled PCF section, and difference of effective index of the two modes is defined as $\Delta n_{\mathrm{eff}}^{\mathrm{m}} = n_{\mathrm{eff}}^{\mathrm{m1}} - n_{\mathrm{eff}}^{\mathrm{m2}}$. The $n_{\mathrm{eff}}^{\mathrm{m1}}$ and $n_{\mathrm{eff}}^{\mathrm{m2}}$ are effective indices of the mode 1 and mode 2 at a certain temperature (T), respectively. An accumulated Φ of 2π means that the local maximum/minimum fringe shifts to the next maximum/minimum fringe. Based on Eq. (1), the wavelength shift ($\mathrm{d}\lambda$) of the proposed device caused by a change in temperature (dT) can be estimated by using the following equation.

$$\frac{1}{\lambda}\frac{\mathrm{d}\lambda}{\mathrm{d}T} = \left[\frac{1}{L}\frac{\mathrm{d}L}{\mathrm{d}T} + \frac{1}{(n_{\mathrm{eff}}^{\mathrm{m1}} - n_{\mathrm{eff}}^{\mathrm{m2}})}\frac{\mathrm{d}(n_{\mathrm{eff}}^{\mathrm{m1}} - n_{\mathrm{eff}}^{\mathrm{m2}})}{\mathrm{d}T}\right] \tag{2}$$

The first term $(1/L)(\mathrm{d}L/\mathrm{d}T)$ in Eq. (2) with the order of 10^{-7} is too small to take into account. Therefore, we can simplify Eq. (2) as below:

$$\frac{\mathrm{d}\lambda}{\lambda}\frac{1}{\mathrm{d}T} = \frac{1}{\Delta n_{\mathrm{eff}}^{\mathrm{m}}}\frac{(n_{\mathrm{eff}}^{\mathrm{m1}\prime} - n_{\mathrm{eff}}^{\mathrm{m2}\prime}) - (n_{\mathrm{eff}}^{\mathrm{m1}} - n_{\mathrm{eff}}^{\mathrm{m2}})}{\mathrm{d}T} \tag{3}$$

The effective index of the interference mode is material-engineered by the liquid which dominates the variation of the wavelength shift ($\mathrm{d}\lambda$) of Eq. (3). Here, $n_{\mathrm{eff}}^{\mathrm{m1}'}$ and $n_{\mathrm{eff}}^{\mathrm{m2}'}$ respectively denote the effective index of the mode 1 and mode 2 for T varying (increasing). The reduction of the effective indices caused by the T variation for the mode 1 and mode 2 are $\Delta n_{\mathrm{eff}}^{\mathrm{m1}} = n_{\mathrm{eff}}^{\mathrm{m1}'} - n_{\mathrm{eff},}^{\mathrm{m1}}$ and $\Delta n_{\mathrm{eff}}^{\mathrm{m2}} = n_{\mathrm{eff}}^{\mathrm{m2}'} - n_{\mathrm{eff}.}^{\mathrm{m2}}$, repectively. Here, the $n_{\mathrm{eff}}^{\mathrm{m1}}$ and $n_{\mathrm{eff}}^{\mathrm{m2}}$ both are negative due to the effective indices decrease when T rises.

Eq. (3) also can be expressed as the following Eq. (4):

$$\frac{\mathrm{d}\lambda}{\lambda}\frac{1}{\mathrm{d}T} = \frac{1}{\Delta n_{\mathrm{eff}}^{\mathrm{m}}}\frac{\Delta n_{\mathrm{eff}}^{\mathrm{m1}} - \Delta n_{\mathrm{eff}}^{\mathrm{m2}}}{\mathrm{d}T} \tag{4}$$

As we can see results in Fig. 6, differential effective indices of the modes: $(\Delta n_{\mathrm{eff}}^{\mathrm{m1}}/\mathrm{d}T) < (\Delta n_{\mathrm{eff}}^{\mathrm{m2}}/\mathrm{d}T)$ that means the term $(\Delta n_{\mathrm{eff}}^{\mathrm{m1}} - \Delta n_{\mathrm{eff}}^{\mathrm{m2}})/\mathrm{d}T < 0$ in Eq. (4) and results in a negative $\mathrm{d}\lambda/\lambda$ as T increases. Therefore, it is inferred that λ shifts toward shorter wavelength side (blue shifts) by the increase of the ambient T for the proposed LC-PCFMI.

Fig. 7 shows the calculation results for the dependence of wavelength shifts caused by the calculated $n_{\mathrm{eff}}^{\mathrm{m}}$-variation with increased T at three designated wavelengths. It is obvious in the consequences that the device has similar sensitivities at different wavelengths but a little more sensitive at shorter wavelengths. From the results of Fig. 7, the proposed sensor with around 30 nm wavelength shift during the T change of 5 °C is achieved to demonstrate a highly T sensitive presentation.

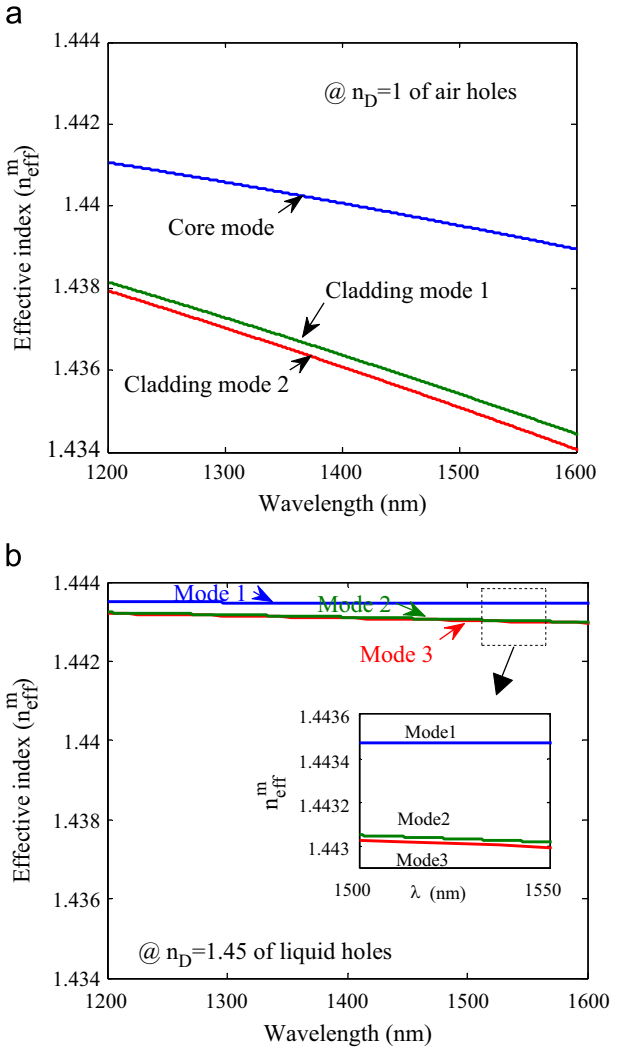

Fig. 4. Effective indices (n_{eff}^{m}) of the three lowest modes for (a) non-filled and (b) liquid-filled conditions.

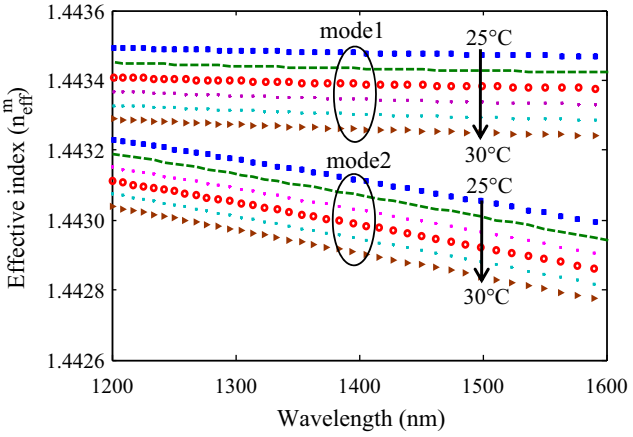

Fig. 5. Effective indices (n_{eff}^{m}) of mode 1 and 2 in the liquid-filled PCF on temperature (T) variations from T=25 °C to 30 °C.

3. Experimental results and discussion

In the measurement, a wide band light source propagated into a circulator, through a piece of SMF, reflected at the LF-PCFMI endface then backed to the SMF and circulator again. The spectral response readouts were directly obtained from an optical spectrum analyzer as

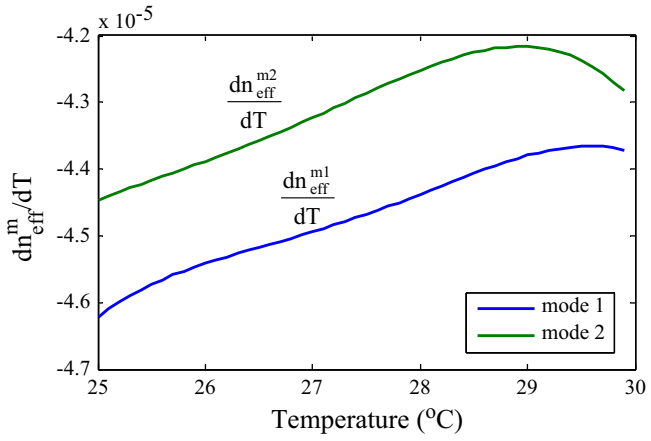

Fig. 6. Dependence of differential effective indices of mode 1 and 2 on temperature at λ=1500 nm.

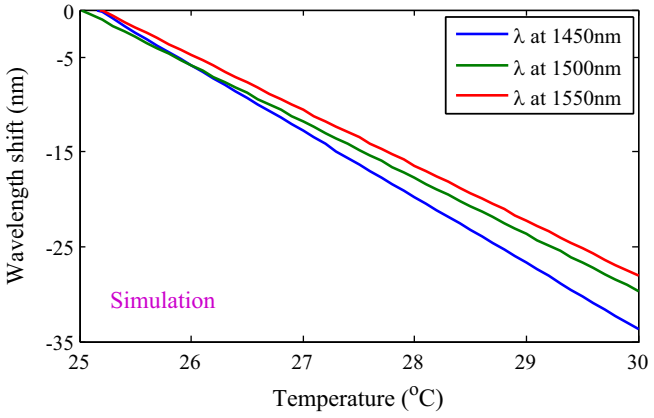

Fig. 7. Calculated temperature sensitivities of wavelength shift for the device at wavelengths of 1450 nm, 1500 nm and 1550 nm, respectively.

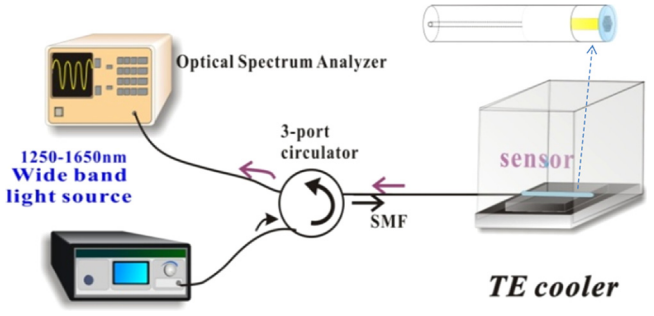

Fig. 8. Experimental setup for the proposed LF-PCFMI.

shown in Fig. 8. The applied T was controlled by a TE cooler and the optical spectra of the liquid-filled PCF varyed with T can be measured. Fig. 9 shows the interference spectra of the LF-PCFMI with liquid-filled parameters of RI with n_D=1.45 and filling length L=31.3 μm of PCF in a temperature range of 25 °C to 30 °C. The experimental results show that λ shifts toward shorter wavelength side when ambient T increases. The agreement of the results between theoretical analysis and experimental measurements also demonstrates the effectiveness of the device.

As expected with the previous inference, experimental results shown in Fig. 9 indicating that λ shifts toward shorter wavelength side (blue shifts) when ambient T increases. The sensitivity for external T of the proposed sensor is so high which is much greater

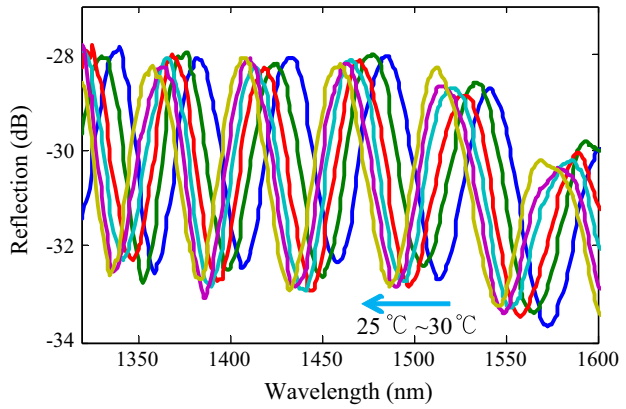

Fig. 9. Experimental interference spectra of the proposed LF-PCFMI when *T* varies.

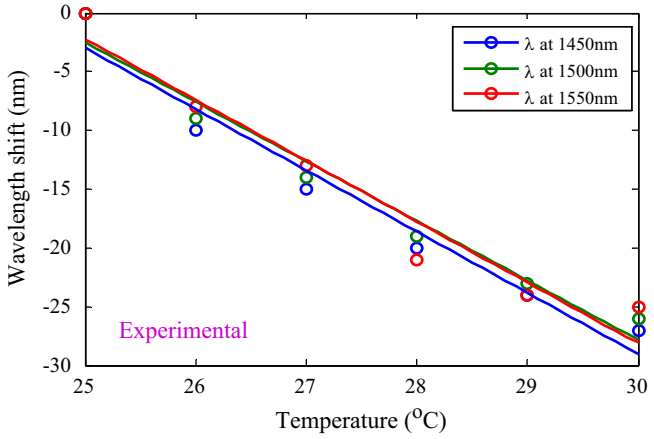

Fig. 10. Measured temperature sensitivities of wavelength shift for the LF-PCFMI at different monitored wavelengths.

than that of the traditional long period fiber grating: LPFG (~0.05 nm/°C) in the air surrounding. Fig. 10 shows the curve fittings of spectral responses, that is to say the sensitivity of the proposed LF-PCFMI, at different wavelengths. As indicated in the results, a very high sensitivity with wavelength shifts of almost 27 nm within temperature variation of 5 °C has been achieved by the proposed sensor.

4. Conclusions

This work has investigated and analyzed a sensitive, ultracompact, tip typed, in-line liquid-filled photonic crystal fiber Michelson interferometer (LF-PCFMI) based on the material dispersion engineering to enhance the sensitivity of temperature. Numerical analysis for the proposed device shows a good agreement with the results of experimental measurement to exhibit the usefulness of the study. The experimental measurement reveals that a high *T* sensitive characteristic has been achieved and their sensitivity can be strongly controlled by filling the leading liquid into the air voids of the PCF. The numerical and experimental results have also verified that the PCF-based sensor with material engineering mechanism can highly modulate the optical properties of the propagating modes.

References

[1] J. Villatoro, V. Finazzi, V.P. Minkovich, V. Pruneri, G. Badenes, Appl. Phys. Lett. 91 (091109) (2007).
[2] R. Jha, J. Villatoro, G. Badenes, Appl. Phys. Lett. 93 (191106) (2008).
[3] L.T. Hsiao, C.P. Yu, Wireless and Optical Communications Conference (WOCC) (2012) 147.
[4] J.M. Hsu, C.L. Lee, P.J. Huang, C.H. Hung, P.Y. Tai, IEEE Photonics Technol. Lett. 24 (2012) 1761.
[5] K. Naeem, B. Kim, J. Han, Y. Chung, Proc. SPIE 8421 (842179) (2012).
[6] H. Liang, W. Zhang, H. Wang, P. Geng, S. Zhang, S. Gao, C. Yang, J. Li, Opt. Lett. 38 (2013) 4019.
[7] T. Han, Y.G. Liu, Z. Wang, Z. Wu, S. Wang, S. Li, Opt. Express 20 (2012) 13320.
[8] Y. Peng, J. Hou, Y. Zhang, Z. Huang, R. Xiao, Q. Lu, Opt. Lett. 38 (2013) 263.
[9] W. Qian, C.L. Zhao, S. He, X. Dong, S. Zhang, Z. Zhang, S. Jin, J. Guo, H. Wei, Opt. Lett. 36 (2011) 1548.
[10] T.T. Alkeskjold, A. Bjarklev, Opt. Lett. 32 (2007) 1707.
[11] S. Mathews, G. Farrell, Y. Semenova, IEEE Photonics Technol. Lett. 23 (2011) 408.
[12] J. Du, Y. Liu, Z. Wang, B. Zou, B. Liu, X. Dong, Opt. Lett. 33 (2008) 2215.
[13] Fang Du, Yan-Qing Lu, Shin-Tson Wu, Appl. Phys. Lett. 85 (2181) (2004).